

Model-Based Real-Time Motion Tracking using Dynamical Inverse Kinematics

Lorenzo Rapetti^{1,2}, Yeshasvi Tirupachuri^{1,3}, Kouros Darvish¹, Claudia Latella¹, Daniele Pucci¹

Abstract—This paper contributes towards the development of motion tracking algorithms for time-critical applications, proposing an infrastructure for solving dynamically the inverse kinematics of human models. We present a method based on the integration of the differential kinematics, and for which the convergence is proved using Lyapunov analysis. The method is tested in an experimental scenario where the motion of a subject is tracked in static and dynamic configurations, and the inverse kinematics is solved both for human and humanoid models. The architecture is evaluated both terms of accuracy and computational load, and compared to iterative optimization algorithms.

I. INTRODUCTION

Nowadays, real-time motion tracking has many established applications in different fields such as medicine, virtual reality, and computer gaming. Moreover, in the field of robotics there is a growing interest in human motion retargeting and imitation [1][2]. Different tracking technologies and algorithms are currently applied. Among these, optical tracking techniques are more spread and have been available since the eighties [3]. Inertial/magnetic tracking technologies have been available only with the advent of micromachined sensors, and ensure higher frequency of data and lower latency, that makes them suited for demanding real-time applications [4]. The objective of motion tracking algorithm is to find the human configuration from a set of measurement. Tracking algorithms can use human body representations with different level of complexity spacing from contours [5][6], stick figure [7][8], and volumes [9][10]. For some techniques it is not required to know *a priori* the shape of the model, and its identification is part of the algorithm [5][7]. When the human is modelled as a kinematic chain, the solution of the model inverse kinematics has a major role in the algorithm [11][12][13][14], hence, strategies to solve it efficiently are required.

Traditionally, in the field of robotics, a common inverse kinematics problem consists in finding the mapping between the end-effector of a manipulator and the corresponding joint configuration. Compared to an industrial manipulator, solving the inverse kinematics for a human kinematic model can be demanding. The human kinematic chain is redundant, it generally has an high number of degrees of freedom (DoF), and may also take into account musculoskeletal constraints

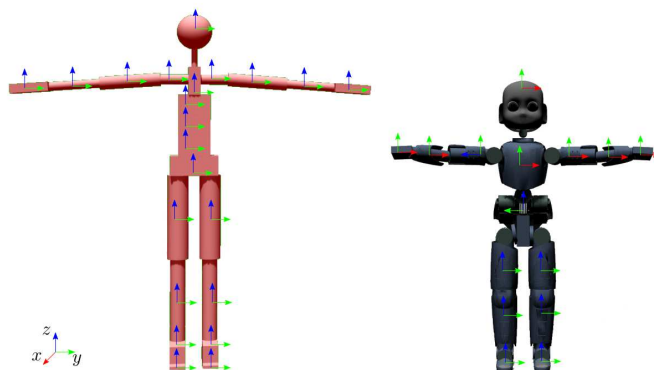


Fig. 1: Model of the human (*left*) and the iCub humanoid robot (*right*) in *T-pose*, with frame definitions of the corresponding physical links.

in order to ensure realistic motion. Moreover, it has to be taken into account the fact that a human is a floating base system, and its configuration space lies on a differentiable manifold [15]. Since finding an analytical closed-form solution for the inverse kinematics of a human model is not always either possible or efficient, a numerical solution is often preferred. One of the most common approach for solving inverse kinematics is to formulate the problem as a non-linear optimization that is solved via iterative algorithms [16][17]. This class of algorithms, referred to as *instantaneous optimization*, aims to converge to a stable solution for each time step. Although instantaneous optimization algorithms converge fast to a solution for common robotics applications, finding the solution for a human model at a sufficient rate for time critical application becomes demanding. In some case, better performance are achieved using heuristic iterative algorithms [18], learning algorithms [19], or combining analytical and numerical methods [20]. An alternative approach consists in rephrasing the inverse kinematics problem as a control problem [21]. This class of algorithms will be referred to as *dynamical optimization* since the model configuration is controlled in order to dynamically converge over time to the desired task space targets. From a computational point of view, the main advantage of this approach consists into the fact that at each time-step the solution is directly computed in a single iteration. The absence of iterations makes the *dynamical optimization* approach faster, and suited for solving whole-body inverse kinematics in motion tracking applications.

This article introduces a scheme for real-time motion tracking using a human, or humanoid, model defined as floating-

¹ Dynamic Interaction Control at Istituto Italiano di Tecnologia, Center for Robotics Technologies, Genova, Italy. (email: name.surname@iit.it)

² Machine Learning and Optimisation, The University of Manchester, Manchester, United Kingdom.

³ DIBRIS, University of Genova, Genova, Italy.

base kinematic chain. The tracking is achieved at high frequency by solving the inverse kinematics using dynamical optimization. The theoretical background for applying dynamical inverse kinematics optimization to floating-base systems is presented using rotation matrix parametrization, and the convergence of the method is proved using Lyapunov theory. The implementation of the proposed scheme is tested with static and dynamical motions, and involving both human and humanoid models. The performance are compared to the results obtained using instantaneous optimization. The paper is organized as following: Section II introduces the notation, the human modeling, and the formulation of the motion tracking as inverse kinematics. Section III presents the theory for applying dynamical optimization inverse kinematics to a floating base models. Section IV lays the experimental details, and in V the results are discussed and compared to instantaneous optimization. Conclusions follow in Section VI.

II. BACKGROUND

A. Notation

- \mathcal{I} denotes an inertial frame of reference.
- $I_{n \times n} \in \mathbb{R}^{n \times n}$ denotes the identity matrix of size n .
- ${}^A p_B \in \mathbb{R}^3$ is the the position of the origin of the frame \mathcal{B} with respect to the frame \mathcal{A} .
- ${}^A R_B \in SO(3)$ represents the rotation matrix of the frames \mathcal{B} with respect to \mathcal{A} .
- ${}^A \omega_B \in \mathbb{R}^3$ is the angular velocity of the frame \mathcal{B} with respect to \mathcal{A} , expressed in \mathcal{A} .
- The operator $\text{tr}(\cdot) : \mathbb{R}^{3 \times 3} \rightarrow \mathbb{R}$ denotes the *trace* of a matrix, such that given $A \in \mathbb{R}^{3 \times 3}$, it is defined as $\text{tr}(A) := A_{1,1} + A_{2,2} + A_{3,3}$.
- The operator $\text{sk}(\cdot) : \mathbb{R}^{3 \times 3} \rightarrow so(3)$ denotes *skew-symmetric* operation of a matrix, such that given $A \in \mathbb{R}^{3 \times 3}$, it is defined as $\text{sk}(A) := (A - A^T)/2$.
- The operator $S(\cdot) : \mathbb{R}^3 \rightarrow so(3)$ denotes *skew-symmetric* vector operation, such that given two vectors $v, u \in \mathbb{R}^3$, it is defined as $v \times u = S(v)u$.
- The *vee* operator $\cdot^\vee : so(3) \rightarrow \mathbb{R}^3$ denotes the inverse of the *skew-symmetric* vector operator, such that given a matrix $A \in so(3)$ and a vector $u \in \mathbb{R}^3$, it is defined as $Au = A^\vee \times u$.
- The operator $\|\cdot\|_2$ indicates the squared norm of a vector, such that given a vector $v \in \mathbb{R}^3$, it is defined as $\|v\|_2 = \sqrt{v_1^2 + v_2^2 + v_3^2}$.

B. Modelling

The human can be modelled as a multi-body mechanical system composed of $n + 1$ rigid bodies, called *links* that are connected by n *joints* with one *degree of freedom* (DoF) each [22]. Additionally, the system is assumed to be *floating base*, i.e. none of the links has an *a priori* constant pose with respect to the inertial frame \mathcal{I} . Hence, a specific frame, attached to a link of the system, is referred to as the *base frame*, and denoted by \mathcal{B} .

The *model configuration* is characterized by the position and the orientation of the *base frame* along with the *joint*

positions. Accordingly, the configuration space lies on the Lie group $\mathbb{Q} = \mathbb{R}^3 \times SO(3) \times \mathbb{R}^n$. An element of the configuration space $q \in \mathbb{Q}$ is defined as the triplet $q = ({}^{\mathcal{I}}p_B, {}^{\mathcal{I}}R_B, s)$ where ${}^{\mathcal{I}}p_B \in \mathbb{R}^3$ and ${}^{\mathcal{I}}R_B \in SO(3)$ denote the position and the orientation of the *base frame* respectively, and $s \in \mathbb{R}^n$ is the joints configuration representing the topology of the mechanical system. The position and orientation of a frame \mathcal{A} attached to the model can be obtained via geometrical forward kinematic map $h_{\mathcal{A}}(\cdot) : \mathbb{Q} \rightarrow (SO(3), \mathbb{R}^3)$ from the *model configuration*. The forward kinematics can be decomposed into position, i.e. ${}^{\mathcal{I}}p_A = h_{\mathcal{A}}^p(q)$, and orientation, i.e. ${}^{\mathcal{I}}R_A = h_{\mathcal{A}}^o(q)$, maps.

The *model velocity* is characterized by the linear and angular velocity of the *base frame* along with the *joint velocities*. Accordingly, the configuration velocity space lies on the group $\mathbb{V} = \mathbb{R}^3 \times \mathbb{R}^3 \times \mathbb{R}^n$. An element of the configuration velocity space $\nu \in \mathbb{V}$ is defined as $\nu = ({}^{\mathcal{I}}v_B, \dot{s})$ where ${}^{\mathcal{I}}v_B = ({}^{\mathcal{I}}\dot{p}_B, {}^{\mathcal{I}}\omega_B) \in \mathbb{R}^6$ denotes the linear and angular velocity of the *base frame*, and \dot{s} denotes the joint velocities. The velocity of a frame \mathcal{A} attached to the model is denoted by ${}^{\mathcal{I}}v_A = ({}^{\mathcal{I}}\dot{p}_A, {}^{\mathcal{I}}\omega_A)$ with the linear and the angular velocity components respectively. The mapping between frame velocity ${}^{\mathcal{I}}v_A$ and configuration velocity ν is achieved through the *Jacobian* $J_A = J_A(q) \in \mathbb{R}^{6 \times (n+6)}$, i.e. ${}^{\mathcal{I}}v_A = J_A(q)\nu$. The *Jacobian* is composed of the linear part $J_A^l(q)$ and the angular part $J_A^a(q)$ that maps respectively the linear and the angular velocities, i.e. ${}^{\mathcal{I}}\dot{p}_A = J_A^l(q)\nu$ and ${}^{\mathcal{I}}\omega_A = J_A^a(q)\nu$.

C. Problem Statement

Motion tracking algorithms aims to find the human configuration given a set of targets describing the kinematics of its links. Those targets are the measurements of the link pose and velocity expressed in a world reference frame, and are retrieved from sensors or image processing. The process of estimating the configuration of a mechanical system from task space measures is generally referred to as inverse kinematics, and can be formulated as follows.

Problem 1. Given a set of n_p frames $\mathcal{P} = \{\mathcal{P}_1, \mathcal{P}_2, \dots, \mathcal{P}_{n_p}\}$ with the associated target position ${}^{\mathcal{I}}p_{\mathcal{P}_i}(t) \in \mathbb{R}^3$ and target linear velocity measurements ${}^{\mathcal{I}}\dot{p}_{\mathcal{P}_i}(t) \in \mathbb{R}^3$, and given a set of n_o frames $\mathcal{O} = \{\mathcal{O}_1, \mathcal{O}_2, \dots, \mathcal{O}_{n_o}\}$ with the associated target orientation ${}^{\mathcal{I}}R_{\mathcal{O}_j}(t) \in SO(3)$ and target angular velocity measurements ${}^{\mathcal{I}}\omega_{\mathcal{O}_j}(t) \in \mathbb{R}^3$, find the state configuration $(q(t), \nu(t))$ of a model such that:

$$\begin{cases} {}^{\mathcal{I}}p_{\mathcal{P}_i}(t) = h_{\mathcal{P}_i}^p(q(t)), & \forall i = 1, \dots, n_p \\ {}^{\mathcal{I}}R_{\mathcal{O}_j}(t) = h_{\mathcal{O}_j}^o(q(t)), & \forall j = 1, \dots, n_o \\ {}^{\mathcal{I}}\dot{p}_{\mathcal{P}_i}(t) = J_{\mathcal{P}_i}^l(q(t))\nu(t), & \forall i = 1, \dots, n_p \\ {}^{\mathcal{I}}\omega_{\mathcal{O}_j}(t) = J_{\mathcal{O}_j}^a(q(t))\nu(t), & \forall j = 1, \dots, n_o \\ As(t) \leq b, \\ C\dot{s}(t) \leq d, \end{cases} \quad (1)$$

where A and b are two parameters that represent the limits for the joint configuration of the model, and C and d represents the limits for the joint velocity.

The following quantities are defined in order to have a compact representation of *Problem 1*. The targets are collected in a *pose target vector* $x(t)$ and *velocity target vector* $v(t)$:

$$x(t) := \begin{bmatrix} \mathcal{I}_{p_{\mathcal{P}_1}}(t) \\ \dots \\ \mathcal{I}_{p_{\mathcal{P}_{n_p}}}(t) \\ \mathcal{I}_{R_{\mathcal{O}_1}}(t) \\ \dots \\ \mathcal{I}_{R_{\mathcal{O}_{n_o}}}(t) \end{bmatrix}, \quad v(t) := \begin{bmatrix} \mathcal{I}_{\dot{p}_{\mathcal{P}_1}}(t) \\ \dots \\ \mathcal{I}_{\dot{p}_{\mathcal{P}_{n_p}}}(t) \\ \mathcal{I}_{\omega_{\mathcal{O}_1}}(t) \\ \dots \\ \mathcal{I}_{\omega_{\mathcal{O}_{n_o}}}(t) \end{bmatrix}, \quad (2)$$

and, forward geometrical kinematic can be expressed as a single vector $h(q(t))$, and Jacobians as single matrix $J(q(t))$:

$$h(q(t)) := \begin{bmatrix} h_{\mathcal{P}_1}^p(q(t)) \\ \dots \\ h_{\mathcal{P}_{n_p}}^p(q(t)) \\ h_{\mathcal{O}_1}^o(q(t)) \\ \dots \\ h_{\mathcal{O}_{n_o}}^o(q(t)) \end{bmatrix}, \quad J(q(t)) := \begin{bmatrix} J_{\mathcal{P}_1}^\ell(q(t)) \\ \dots \\ J_{\mathcal{P}_{n_p}}^\ell(q(t)) \\ J_{\mathcal{O}_1}^a(q(t)) \\ \dots \\ J_{\mathcal{O}_{n_o}}^a(q(t)) \end{bmatrix}, \quad (3)$$

the set of equations in (1) can then be reduced, using the definitions of (2) and (3), to the following two equations describing respectively the *forward kinematics* and *differential kinematics* for all the target frames:

$$x(t) = h(q(t)), \quad (4a)$$

$$v(t) = J(q(t))\nu(t). \quad (4b)$$

As mentioned in Section I, in the case of highly articulated systems, like humans, finding an analytical solution to Equation (4) is often vain, and a numerical optimization solution is preferred. Hence, distance measurements used in the optimization problem have to be defined. The distances between a given state $q(t)$ and the pose targets $x(t)$ are collected in a residual vector $r(q(t), x(t))$ defined as follow:

$$r(q(t), x(t)) = \begin{bmatrix} \mathcal{I}_{p_{\mathcal{P}_1}}(t) - h_{\mathcal{P}_1}^p(q(t)) \\ \dots \\ \mathcal{I}_{p_{\mathcal{P}_{n_p}}}(t) - h_{\mathcal{P}_{n_p}}^p(q(t)) \\ \text{sk}(h_{\mathcal{O}_1}^o(q(t))^T \mathcal{I}_{R_{\mathcal{O}_1}}(t))^\vee \\ \dots \\ \text{sk}(h_{\mathcal{O}_{n_o}}^o(q(t))^T \mathcal{I}_{R_{\mathcal{O}_{n_o}}}(t))^\vee \end{bmatrix}. \quad (5)$$

Traditionally, Euler angles or unit quaternion parametrization are used in literature while defining the distance for link orientations. However, using rotation matrix parametrization, we use the $\text{sk}(\cdot)^\vee$ operator for defining the distance. The motivation behind the choice of this operator is in the prove of convergence presented in Appendix. The distances from the target velocities $v(t)$ are collected in the velocity residual vector $u(q(t), \nu(t), v(t))$ defined as:

$$u(q(t), \nu(t), v(t)) = v(t) - J(q(t))\nu(t). \quad (6)$$

III. DYNAMICAL OPTIMIZATION METHOD

The dynamical optimization method aims to minimize the residual vectors, whose dynamics is described by the differential equations (5) and (6), by controlling the state configuration $(q(t), \nu(t))$. The block diagram of the method is presented in Figure 2. The scheme is composed by three main parts: a) correction of velocity targets to ensure convergence of pose targets, b) inversion of the model differential kinematics to obtain the state velocity $\nu(t)$, and c) integration of state velocity to obtain the configuration $q(t)$.

A. Velocity Correction

At this stage, we assume the state velocity $\nu(t)$ is the input to a dynamical system, and we want to control the system in order to drive the residual vectors towards zero.

Lemma 1. Assume $r(q(t), x(t))$ defined as in (5), $u(q(t), \nu(t), v(t))$ defined as in (6), and the system

$$u(q(t), \nu(t), v(t)) + Kr(q(t), x(t)) = 0, \quad (7)$$

where $K \in \mathbb{R}^{(3n_p+3n_o)} \times \mathbb{R}^{(3n_p+3n_o)}$ is a positive definite diagonal matrix. Then, $(r, u) = (0, 0)$ denotes an (almost) globally asymptotically stable equilibrium point for the system.

The proof is provided in appendix. *Lemma 1* shows that we can control the system input $\nu(t)$ so that $r(t)$ and $u(t)$ converge to zero for (almost) any initialization $q(t_0)$. Replacing the expression of $u(q(t), \nu(t))$, presented in (6), in the system (7), it can be observed that the expression is linear in state velocity $\nu(t)$.

$$J(q(t))\nu(t) = v(t) + Kr(q(t), x(t)). \quad (8)$$

The rate of convergence depends on the magnitude of the elements of matrix K . Higher values of K imply faster convergence of the system (7) towards zero. However, the implementation of discrete time solution bounds the values of K depending on the sampling time [23]. In fact, Equation (8) is solved for a discrete control input $\nu(t_k)$ from the following equation:

$$J(q(t_{k-1}))\nu(t_k) = v(t_k) + Kr(q(t_{k-1}), x(t_k)). \quad (9)$$

The way the discrete control input $\nu(t_k)$ is obtained will be discussed in III-B. It is interesting to notice that the Equation (8) establishing the control input law, is equivalent to a differential kinematic equation (4b) where the target velocity vector $v(t)$ is replaced by a corrected target velocity vector $v^*(t) := v(t) + Kr(q(t), x(t))$.

B. Inverse Differential Kinematics

The inverse differential kinematics is the problem of inverting the differential kinematic Equation (4b) in order to find the configuration state velocity $\nu(t)$ for a given set of task space velocities. Computing control input $\nu(t_k)$ from (9) is equivalent to solving the inverse differential kinematics for the corrected target velocity $v^*(t_k)$. The solution depends on the rank of the Jacobian matrix $J(q(t_k))$, and in most of the

cases it is found numerically. Being it a common problem to most of the inverse kinematics methods [16][17][21][24], different strategies can be found in literature. Among the possible solutions, a common approach is to use Jacobian generalized inverse [25]. In order to take into account also the model constraints, an alternative approach is to solve it via QP optimization:

$$\underset{\nu(t_k)}{\text{minimize}} \quad \|\nu^*(t_k) - J(q(t_{k-1}))\nu(t_k)\|_2 \quad (10a)$$

$$\text{subject to} \quad G\nu(t_k) \leq g \quad (10b)$$

where G and g are two parameters used for limits avoidance that depend on $q(t_{k-1})$ and the model constraints parameters A , b , C and d .

C. Numerical Integration

Given the configuration velocity solution $\nu(t_k)$, it is possible to compute the state configuration $q(t_k)$ by defining an initial configuration $q(t_0)$ and integrating over time. Base position ${}^{\mathcal{I}}p_B$ and joints configuration s lie in vector space over \mathbb{R} for which most of the numerical integrations methods proposed in literature can be used [26]. The integration of the base angular velocity ${}^{\mathcal{I}}\omega_B(t_k)$ is not trivial, numerical integration errors can lead to the violation of the orthonormality condition [27] for the base orientation ${}^{\mathcal{I}}R_B$. A possible approach presented in literature is the Baumgarte stabilization [27], the convergence of ${}^{\mathcal{I}}R_B(t_k)$ over $SO(3)$ is ensured computing the base orientation matrix dynamics ${}^{\mathcal{I}}\dot{R}_B(t_k) \in \mathbb{R}^{3 \times 3}$ as follow:

$$A(t_{k-1}) = \rho({}^{\mathcal{I}}R_B(t_{k-1})^T {}^{\mathcal{I}}R_B(t_{k-1}))^{-1} - I_{3 \times 3}, \quad (11a)$$

$${}^{\mathcal{I}}\dot{R}_B(t_k) = (S({}^{\mathcal{I}}\omega_B(t_k)) + A(t_{k-1})) {}^{\mathcal{I}}R_B(t_{k-1}), \quad (11b)$$

where $\rho \in \mathbb{R}^+$ is the gain regulating the convergence towards the orthonormality condition, and $\Delta t_k = t_k - t_{k-1}$ is the time step. The advantage of obtaining the configuration $q(t_k)$ trough integration of velocity $\nu(t_k)$ is that the two estimated quantities are directly related, and continuity of the state configuration is ensured.

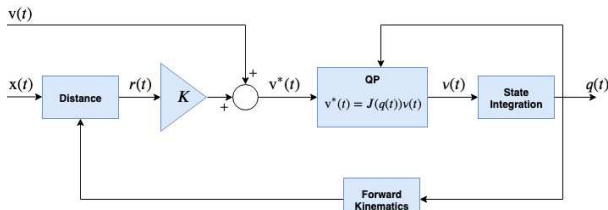


Fig. 2: Dynamical optimization algorithm for real-time inverse kinematics of floating base model.

IV. EXPERIMENTS

A. Motion Data Acquisition

The proposed method has been implemented and tested using motion data acquired with the Xsens Awinda wearable suit [28] providing pose and velocity of a 23 links human model, computed from a set of distributed Inertial Measurement Units (IMUs). The motion data is streamed through

YARP middleware [29] that facilitates recording and real-time playback of data. The motion data is acquired for three scenarios with different levels of dynamicity: *t-pose* where the subject stands on two feet with the arms parallel to the ground, *walking* where the subject walks on a treadmill at a constant speed of 4 Km/h, and *running* where the subject runs on a treadmill at a constant speed of 10 Km/h.

B. Models

The motion tracking is performed by using two different human models defined as in II-B. Both the models are composed by 23 *physical links* representing segments of the human body. Each physical link is attached to the next one trough a certain number of rotational joint connected trough *dummy links*, i.e. links with dimension zero, in order to model human joints with multiple DoFs. In one human model (*Human66*) all the physical links are connected through spherical joints (3 rotational joints), i.e. a total of 66 DoFs and 67 links. The second model (*Human48*) is based on the modelling of the human musculoskeletal system as described in clinical studies [30][31][32], it has a reduced number of joint, i.e. 48DoFs, and takes into account human joint limits.

Additionally, we consider experiments with a model of the *iCub* humanoid robot [33]. The motivation behind this is to highlight the performance in achieving motion tracking, and motion retargeting from the human to a humanoid. The *iCub* model is composed of 15 physical links connected through 34 rotational joints, with joint limits defined accordingly to the real robot mechanic constraints.

The definition of link frames for the human model and the robot model is highlighted in Figure 1. Considering that all the models have only rotational joints, the inverse kinematics problem is defined with a rotational and angular velocity target for each physical link, i.e. $n_o = 23$ for the human model and $n_o = 15$ for the humanoid model. Additionally, as both the models are floating base, a position and linear velocity target is used for the base frame, i.e. $n_p = 1$.

V. RESULTS

The performance of dynamical optimization inverse kinematics solver is compared to instantaneous optimization implementations. The evaluation is done in terms of computational load and accuracy on a 2.3GHz Intel Core i7 processor with 16GB of RAM. The accuracy is measured with two metrics, one for the orientation targets and one for the velocity targets. The *mean normalized trace error (MNTE)* is a dimensionless metric measuring the overall accuracy of the orientation targets:

$$MNTE = \frac{1}{n_o} \sum_{j=1}^{n_o} \frac{\text{tr}(I_{3 \times 3} - {}^{\mathcal{I}}\hat{R}_{\mathcal{O}_j}(q)^T {}^{\mathcal{I}}R_{\mathcal{O}_j})}{2}, \quad (12)$$

where ${}^{\mathcal{I}}\hat{R}_{\mathcal{O}_j}(q)$ is the frame orientation given the state q , and the $\frac{1}{2}$ factor normalize the value of the trace between 0 and

1. For the angular velocities, the overall error is evaluated as *root mean squared error (RMSE)*:

$$RMSE = \sqrt{\frac{1}{n_o} \sum_{j=1}^{n_o} \frac{\|\mathcal{I}\omega_{\mathcal{O}_j} - \mathcal{I}\hat{\omega}_{\mathcal{O}_j}(q, \nu)\|_2^2}{3}}, \quad (13)$$

where $\hat{\omega}_{\mathcal{O}_j}(q, \nu)$ is the frame velocity given the configuration (q, ν) . The computational load is evaluated as the time for computing the state (q, ν) . The statistics have been collected discarding the transient of 2 second from the initial time t_0 , and the results are shown in Figure 4.

A. Instantaneous Optimization

As mentioned in Section I, the instantaneous optimization methods solve the inverse kinematics at each time-step t_k through non-linear optimization. A general formulation of the optimization problem is defined as following:

$$\underset{q(t_k)}{\text{minimize}} \quad \|K_r r(q(t_k), x(t_k))\|_2 \quad (14a)$$

$$\text{subject to} \quad As(t_k) \leq b \quad (14b)$$

where K_r is a weight matrix that matches the unit measurements of targets distances, and eventually assigns a weight to each of the target. A common approach for solving the non-linear optimization problem is to consider the linear approximation of the system by recalling the Jacobian matrix definition, and solve the problem iteratively [34][35]. However, in order to enforce state configuration constraints, recent approaches make also use of convex optimization [24][36]. As benchmark, we have implemented instantaneous inverse kinematics optimization using iDynTree [37] multibody kinematics library, and the IPOPT software library for non-linear optimization [38]. The stopping criteria for the optimization is the *pose error* accuracy, and it has been tuned in order to find a solution in a time comparable to the dynamical optimization. Two different implementations have been tested. The first one, referred to as *whole-body optimization*, solves a single optimization problem instantiated for the whole-system. Instead, the second implementation instantiate the optimization process dividing the model into multiple subsystems, each consisting of exactly a pair of targets, and solves the subproblems in parallel. We refer to this implementation as *pair-wise optimization*.

The solution for the state velocity $\nu(t_k)$ comes from an optimization problem formulated as follow:

$$\underset{\nu(t_k)}{\text{minimize}} \quad \|K_u u(q(t_k), \nu(t_k), v(t_k))\|_2 \quad (15a)$$

$$\text{subject to} \quad C\dot{s}(t_k) \leq d \quad (15b)$$

where K_u is a weight matrix that matches the unit measurements of targets distances, and eventually assigns a weight to each of the target. In case of state velocity, it can be observed that there is a linear relationship with the velocity target vector as expressed by the differential kinematics Equation (4b). Hence, given $q(t_k)$ obtained as output of the optimization problem (14), the state velocity is the result of

the inverse differential kinematics described in Section III-B and is obtained using OSQP library [39].

Looking at Figure 4, it can be observed that the performance of instantaneous optimization approaches decrease as the task gets more dynamic. This is particularly evident for the computational time. In the whole-body optimization, not only the average computational time increase, it is characterized by a large variance, reaching peaks above $25ms$ during the running task. Concerning the pair-wised optimization, the increase of time between walking and running is less evident. However, the pair-wised optimization takes longer for finding a solution for the iCub model because of the local difference between the human and the robot kinematics.

B. Dynamical Optimization

The *dynamical optimization* inverse kinematics has been implemented using iDynTree [37] multibody kinematics library, and the inverse differential kinematics is solved making use of OSQP [39]. Figure 3 highlights the rate of convergence of the error from a given initial zero configuration ($s(0) = 0$) towards a target static pose. When the gain is zero, there is no velocity correction and the error remains constant. However, increasing the magnitude of K , the error converges to its steady state value in less then one second. A large value of the gain K leads to system instability as mentioned in III-A.

From Figure 4, the *dynamical optimization* orientation error is always comparable with the results achieved with *instantaneous optimization*. The only case in which it shows worst orientation accuracy is with the *Human66* model during running task. Concerning the angular velocity error, the performances are again comparable during dynamic motion, while it is higher for the t-pose with the constrained models. This angular velocity error may be due to the fact that a corrected angular velocity is used in place of the measured link angular velocities, and the joint constraints may introduce a constant constraint error because of an unfeasible configuration. Concerning the computational load, this method seems to outperform the others not only in terms of a mean computational time, having an average always below $3ms$, but also for its consistency in different scenario.

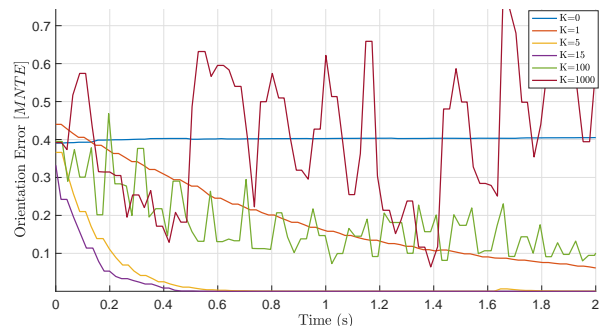


Fig. 3: Convergence of the dynamical inverse kinematics optimization method for a static *T-pose* on a 66 DoF model, starting from a zero configuration. The convergence depends on the magnitude of the gain K .

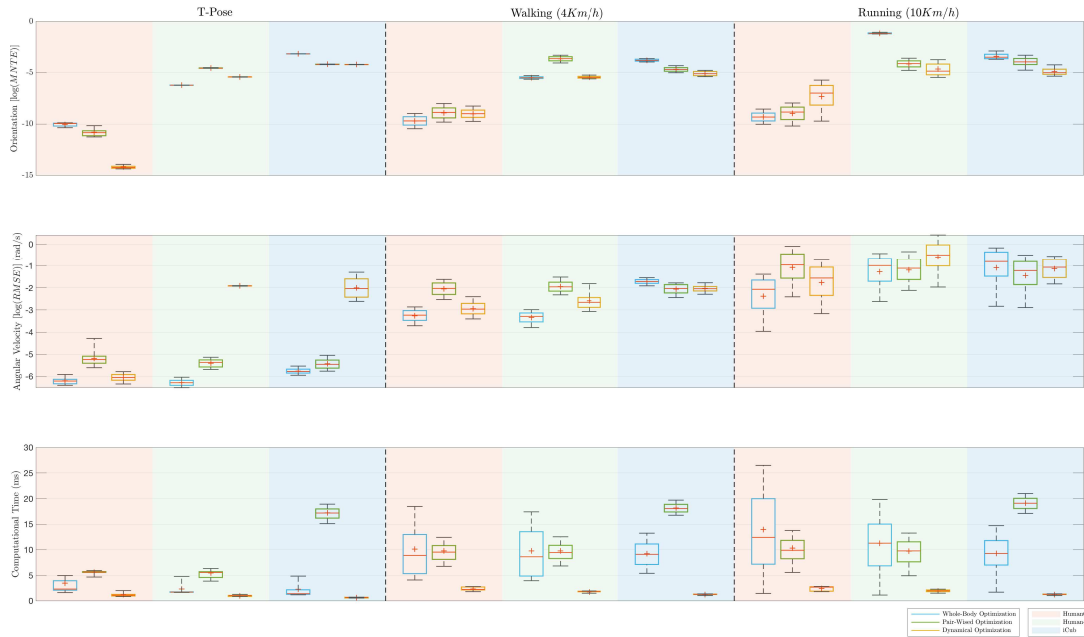


Fig. 4: Comparison of the performance of inverse kinematics methods (*whole-body*, *pair-wise*, and *dynamical*) for three models (two humans, and iCub humanoid) in three different scenarios (*T-pose*, *Walking*, and *Running*). Each line contains the boxplots for a different performance evaluation metric, on the top the overall error for the orientation targets as base 10 logarithm of *mean normalized trace error*, in the middle line the overall error for the angular velocities as base 10 logarithm of *root mean squared error*, and at the bottom the computational time. Logarithmic metrics allows to compare metrics characterized by different order of magnitude in the different scenarios.

VI. CONCLUSIONS

This paper propose an infrastructure for whole-body inverse kinematics of floating-base articulated models in real-time motion tracking applications. The theory is presented using rotation matrix parametrization of orientations, together with the proof of convergence through Lyapunov analysis. The proposed method has been implemented and the performances tested in an experimental scenario with different conditions. Differently from iterative algorithms, the *dynamical optimization* requires a single iteration at each time step keeping the computational time constant, and ensures fast convergence of the error over time. Furthermore, the integration of velocities ensures obtaining a continuous and smooth solution. Its characteristics make it suitable for time-critical motion tracking applications with highly dynamic motions, where iterative algorithms may not converge in a sufficient time. As a future work, the evaluation may be extended to a wider number of algorithms, models, and experimental scenario. Another interesting future work may be the extension of the method to include the dynamic of the system.

ACKNOWLEDGMENTS

This work is supported by Honda R&D Co., Ltd and by EU An.Dy Project that received funding from the European Unions Horizon 2020 research and innovation programme under grant agreement No. 731540. The content of this publication is the sole responsibility of the authors. The European Commission or its services cannot be held responsible for any use that may be made of the information it contains.

APPENDIX: PROOF OF LEMMA 1.

The system in (7) can be written as follow:

$$\begin{bmatrix} u_{\mathcal{P}_i}^p(t) \\ \dots \\ u_{\mathcal{P}_{n_p}}^p(t) \\ u_{\mathcal{O}_1}^o(t) \\ \dots \\ u_{\mathcal{O}_{n_o}}^o(t) \end{bmatrix} + \begin{bmatrix} K_1^p r_{\mathcal{P}_1}^p(t) \\ \dots \\ K_{n_p}^p r_{\mathcal{P}_{n_p}}^p(t) \\ K_1^o r_{\mathcal{O}_1}^o(t) \\ \dots \\ K_{n_o}^o r_{\mathcal{O}_{n_o}}^o(t) \end{bmatrix} = 0, \quad (16)$$

where $r_{\mathcal{P}_i}^p(t) = \mathcal{I}_{p_{\mathcal{P}_i}}(t) - h_{\mathcal{P}_i}^p(q(t))$, $r_{\mathcal{O}_j}^o(t) = \text{sk}(h_{\mathcal{O}_j}^o(q(t))^T \mathcal{I}_{R_{\mathcal{O}_j}}(t))^\vee$, $u_{\mathcal{P}_i}^p(t) = \mathcal{I}_{\mathcal{P}_i}(t) - J_{\mathcal{P}_i}^p(q(t))\nu(t)$, $u_{\mathcal{O}_j}^o(t) = \mathcal{I}_{\omega_{\mathcal{O}_j}}(t) - J_{\mathcal{O}_j}^o(q(t))\nu(t)$, K_i^p and K_j^o are $\mathbb{R}^3 \times \mathbb{R}^3$ blocks on the diagonal of K . This system can be decomposed in to a set of $n_p + n_o$ independent systems, one for each target, depending on the type of target, each subsystem is described by one of the following two equation:

$$u_{\mathcal{P}_i}^p(t) + K_i^p r_{\mathcal{P}_i}^p(t) = 0, \quad (17a)$$

$$u_{\mathcal{O}_j}^o(t) + K_j^o r_{\mathcal{O}_j}^o(t) = 0. \quad (17b)$$

The system (17a) is a linear first order autonomous system, and for K_i positive definite the equilibrium point $(r_{\mathcal{P}_i}^p, u_{\mathcal{P}_i}^p) = (0, 0)$ is globally asymptotically stable. For the system (17b) it can be proved that the equilibrium $(r_{\mathcal{O}_j}^o, u_{\mathcal{O}_j}^o) = (0, 0)$ is an almost globally asymptotically stable equilibrium point [40]. The almost global asymptotically stability of all the subsystems is indeed proved for the point $(r, u) = (0, 0)$, thus the almost globally asymptotically stability of the equilibrium $(r, u) = (0, 0)$ for the system (7) is proved.

REFERENCES

- [1] B. Dariush, M. Gienger, A. Arumbakkam, C. Goerick, Youding Zhu, and K. Fujimura, "Online and markerless motion retargeting with kinematic constraints," in *2008 IEEE/RSJ International Conference on Intelligent Robots and Systems*, Sep. 2008, pp. 191–198.
- [2] X. B. Peng, P. Abbeel, S. Levine, and M. van de Panne, "Deepmimic: Example-guided deep reinforcement learning of physics-based character skills," *ACM Trans. Graph.*, vol. 37, no. 4, pp. 143:1–143:14, Jul. 2018. [Online]. Available: <http://doi.acm.org/10.1145/3197517.3201311>
- [3] J. K. Aggarwal and Q. Cai, "Human motion analysis: A review," *Computer vision and image understanding*, vol. 73, no. 3, pp. 428–440, 1999.
- [4] R. Zhu and Z. Zhou, "A real-time articulated human motion tracking using tri-axis inertial/magnetic sensors package," *IEEE Transactions on Neural systems and rehabilitation engineering*, vol. 12, no. 2, pp. 295–302, 2004.
- [5] A. Shio and J. Sklansky, "Segmentation of people in motion," in *Proceedings of the IEEE Workshop on Visual Motion*, Oct 1991, pp. 325–332.
- [6] M. K. Leung and Yee-Hong Yang, "First sight: A human body outline labeling system," *IEEE Transactions on Pattern Analysis and Machine Intelligence*, vol. 17, no. 4, pp. 359–377, April 1995.
- [7] Niyogi and Adelson, "Analyzing and recognizing walking figures in xyt," in *1994 Proceedings of IEEE Conference on Computer Vision and Pattern Recognition*, June 1994, pp. 469–474.
- [8] A. G. Bharatkumar, K. E. Daigle, M. G. Pandey, Qin Cai, and J. K. Aggarwal, "Lower limb kinematics of human walking with the medial axis transformation," in *Proceedings of 1994 IEEE Workshop on Motion of Non-rigid and Articulated Objects*, Nov 1994, pp. 70–76.
- [9] S. Wachter and H.-H. Nagel, "Tracking persons in monocular image sequences," *Computer Vision and Image Understanding*, vol. 74, no. 3, pp. 174–192, 1999.
- [10] J. Gall, C. Stoll, E. De Aguiar, C. Theobalt, B. Rosenhahn, and H.-P. Seidel, "Motion capture using joint skeleton tracking and surface estimation," in *2009 IEEE Conference on Computer Vision and Pattern Recognition*. IEEE, 2009, pp. 1746–1753.
- [11] J.-S. Monzani, P. Baerlocher, R. Boulic, and D. Thalmann, "Using an intermediate skeleton and inverse kinematics for motion retargeting," in *Computer Graphics Forum*, vol. 19, no. 3. Wiley Online Library, 2000, pp. 11–19.
- [12] G. Pons-Moll, A. Baak, J. Gall, L. Leal-Taixe, M. Mueller, H.-P. Seidel, and B. Rosenhahn, "Outdoor human motion capture using inverse kinematics and von mises-fisher sampling," in *2011 International Conference on Computer Vision*. IEEE, 2011, pp. 1243–1250.
- [13] V. Ganapathi, C. Plagemann, D. Koller, and S. Thrun, "Real time motion capture using a single time-of-flight camera," in *2010 IEEE Computer Society Conference on Computer Vision and Pattern Recognition*. IEEE, 2010, pp. 755–762.
- [14] A. Aristidou and J. Lasenby, "Motion capture with constrained inverse kinematics for real-time hand tracking," in *2010 4th International Symposium on Communications, Control and Signal Processing (ISCCSP)*. IEEE, 2010, pp. 1–5.
- [15] S. Traversaro and A. Saccon, "Multibody dynamics notation," *Technische Universiteit Eindhoven, Tech. Rep.*, 2016.
- [16] A. Goldenberg, B. Benhabib, and R. Fenton, "A complete generalized solution to the inverse kinematics of robots," *IEEE Journal on Robotics and Automation*, vol. 1, no. 1, pp. 14–20, March 1985.
- [17] S. R. Buss, "Introduction to inverse kinematics with jacobian transpose, pseudoinverse and damped least squares methods," *IEEE Journal of Robotics and Automation*, vol. 17, no. 1-19, p. 16, 2004.
- [18] A. Aristidou and J. Lasenby, "Fabrik: A fast, iterative solver for the inverse kinematics problem," *Graphical Models*, vol. 73, no. 5, pp. 243–260, 2011.
- [19] K. Grochow, S. L. Martin, A. Hertzmann, and Z. Popović, "Style-based inverse kinematics," in *ACM transactions on graphics (TOG)*, vol. 23, no. 3. ACM, 2004, pp. 522–531.
- [20] D. Tolani, A. Goswami, and N. I. Badler, "Real-time inverse kinematics techniques for anthropomorphic limbs," *Graphical Models*, vol. 62, no. 5, pp. 353 – 388, 2000. [Online]. Available: <http://www.sciencedirect.com/science/article/pii/S1524070300905289>
- [21] L. Sciavicco and B. Siciliano, "A solution algorithm to the inverse kinematic problem for redundant manipulators," *IEEE Journal on Robotics and Automation*, vol. 4, no. 4, pp. 403–410, 1988.
- [22] C. Latella, M. Lorenzini, M. Lazzaroni, F. Romano, S. Traversaro, M. A. Akhras, D. Pucci, and F. Nori, "Towards real-time whole-body human dynamics estimation through probabilistic sensor fusion algorithms," *Autonomous Robots*, pp. 1–13, 2018.
- [23] K. Ogata et al., *Discrete-time control systems*. Prentice Hall Englewood Cliffs, NJ, 1995, vol. 2.
- [24] O. Kanoun, F. Lamiroux, and P. Wieber, "Kinematic control of redundant manipulators: Generalizing the task-priority framework to inequality task," *IEEE Transactions on Robotics*, vol. 27, no. 4, pp. 785–792, Aug 2011.
- [25] C. R. Rao, S. K. Mitra et al., "Generalized inverse of a matrix and its applications," in *Proceedings of the Sixth Berkeley Symposium on Mathematical Statistics and Probability, Volume 1: Theory of Statistics*. The Regents of the University of California, 1972.
- [26] P. J. Davis and P. Rabinowitz, *Methods of numerical integration*. Courier Corporation, 2007.
- [27] S. Gros, M. Zanon, and M. Diehl, "Baumgarte stabilisation over the so(3) rotation group for control," in *2015 54th IEEE Conference on Decision and Control (CDC)*, Dec 2015, pp. 620–625.
- [28] D. Roetenberg, H. Luinge, and P. Slycke, "Xsens MVN: Full 6dof human motion tracking using miniature inertial sensors." [Online]. Available: <http://human.kyst.com.tw/upload/downloads/46130703234558070.pdf>
- [29] G. Metta, P. Fitzpatrick, and L. Natale, "Yarp: yet another robot platform," *International Journal of Advanced Robotic Systems*, vol. 3, no. 1, p. 8, 2006.
- [30] J. Moll and V. Wright, "Normal range of spinal mobility. an objective clinical study," *Annals of the rheumatic diseases*, vol. 30, no. 4, p. 381, 1971.
- [31] J. Gerhardt, "Clinical measurements of joint motion and position in the neutral-zero method and sft recording: basic principles," *International rehabilitation medicine*, vol. 5, no. 4, pp. 161–164, 1983.
- [32] M. Alison Middleditch, M. Jean Oliver et al., *Functional anatomy of the spine*. Elsevier Health Sciences, 2005.
- [33] L. Natale, C. Bartolozzi, D. Pucci, A. Wykowska, and G. Metta, "icub: The not-yet-finished story of building a robot child," *Science Robotics*, vol. 2, no. 13, p. eaaq1026, 2017.
- [34] J. Barnes, "An algorithm for solving non-linear equations based on the secant method," *The Computer Journal*, vol. 8, no. 1, pp. 66–72, 1965.
- [35] R. Fletcher, "Generalized Inverse Methods for the Best Least Squares Solution of Systems of Non-Linear Equations," *The Computer Journal*, vol. 10, no. 4, pp. 392–399, 02 1968.
- [36] F. Blanchini, G. Fenu, G. Giordano, and F. A. Pellegrino, "A convex programming approach to the inverse kinematics problem for manipulators under constraints," *European Journal of Control*, vol. 33, pp. 11–23, 2017.
- [37] F. Nori, S. Traversaro, J. Eljaik, F. Romano, A. Del Prete, and D. Pucci, "icub whole-body control through force regulation on rigid noncoplanar contacts," *Frontiers in Robotics and AI*, vol. 2, no. 6, 2015.
- [38] A. Wächter and L. T. Biegler, "On the implementation of an interior-point filter line-search algorithm for large-scale nonlinear programming," *Mathematical Programming*, vol. 106, no. 1, pp. 25–57, Mar 2006.
- [39] B. Stellato, G. Banjac, P. Goulart, A. Bemporad, and S. Boyd, "OSQP: An operator splitting solver for quadratic programs," *ArXiv e-prints*, Nov. 2017.
- [40] R. Olfati-Saber, "Nonlinear control of underactuated mechanical systems with application to robotics and aerospace vehicles," Ph.D. dissertation, Massachusetts Institute of Technology, 2001.